Physics and Chemistry of Minerals (2024) 51:38
https://doi.org/10.1007/s00269-024-01297-2

ORIGINAL PAPER

High pressure and high temperature Brillouin scattering measurements of pyrope single crystals using flexible CO_2 laser heating systems

A. Kurnosov[1] · G. Criniti[1,2] · T. Boffa Ballaran[1] · H. Marquardt[3] · D. J. Frost[1]

Received: 17 July 2024 / Accepted: 12 September 2024 / Published online: 15 October 2024

Abstract
Single-crystal Brillouin scattering measurements are important for interpreting seismic velocities within the Earth and other planetary interiors. These measurements are rare, however, at temperatures above 1000 K, due to the fact that the transparent samples cannot be heated by common laser heating systems operating at a wavelength on the order of 1 µm. Here we present Brillouin scattering data on pyrope collected at pressures up to 23.8 GPa and temperatures between 850 and 1900 K using a novel CO_2 laser heating system confined in either a flexible hollow silica waveguide or an articulated arm with mirrors mounted in each junction to direct the laser to the exit point. Pyrope has been chosen because it has been extensively studied at high pressures and moderate temperatures and therefore it is an excellent sample for benchmarking the CO_2 laser heating system. The new high-temperature velocity data collected in this study allow the room pressure thermal parameters of pyrope to be constrained more tightly, resulting in values that reproduce the temperature dependence of the unit-cell volume of pyrope measured in recent studies at ambient pressure. Aggregate wave velocities of pyrope calculated along an adiabat using the thermoelastic parameters determined in this study are larger than those obtained using published values, implying that velocities for many mantle components may be underestimated at mantle temperatures because high temperature experimental data are lacking.

Keywords Single-crystal Brillouin scattering · CO_2 laser heating · Pyrope · High-pressure high-temperature elasticity

Introduction

Aluminosilicate garnet is a major mineral throughout the Earth's upper mantle and transition zone and is present within the top 100 km of the lower mantle (Bass and Anderson 1984; Irifune and Ringwood 1987; Weidner and Ito 1987; Duffy and Anderson 1989). Within a bulk silicate Earth (BSE) composition, the most dominant component of aluminosilicate garnet is pyrope, $Mg_3Al_2Si_3O_{12}$, which therefore plays a major role in determining mantle seismic velocities to depths of approximately 700 km. While the elastic properties of pyrope have been extensively studied, (see Angel et al. 2022; for a comprehensive review), there is, however, still disagreement among these studies, especially in terms of the pressure and temperature derivatives of the bulk and shear moduli. Lu et al. (2013) used Brillouin scattering measurements performed in the diamond anvil cell (DAC) to examine the elastic properties of Fe-bearing pyrope but due to the use of an external resistive heater, the highest temperature data were only collected at 750 K. At such conditions, the temperature derivatives cannot be determined with sufficient accuracy to allow extrapolation to mantle temperatures without significant uncertainties. Similarly, the three studies performed on pyrope in the multi-anvil apparatus using ultrasonic-measurements are in poor agreement at room temperature (Gwanmesia et al. 2006, 2007; Zou et al. 2012; Chantel et al. 2016) and although the agreement actually improves for the higher

✉ A. Kurnosov
Alexander.Kurnosov@uni-bayreuth.de

[1] Bayerisches Geoinstitut, Universität Bayreuth, 95447 Bayreuth, Germany

[2] Earth and Planets Laboratory, Carnegie Institution for Science, Washington, DC 20015, USA

[3] Department of Earth Sciences, University of Oxford, Oxford OX1 3AN, UK

temperature data, the resulting temperature derivatives are quite different. As few data points were collected in these studies above 1300 K, the results still need to be extrapolated to reach actual mantle temperatures. A major objective in mineral physics is to be able to discern whether variations in mantle seismic wave velocities have chemical or thermal origins (Duffy and Anderson 1989; Cammarano and Romanowicz 2007). At the base of the transition zone, current pyrope elasticity models (Stixrude and Lithgow-Bertelloni 2005; Zou et al. 2012; Chantel et al. 2016) deviate from each other in their predicted values of shear, v_S, and compressional, v_P, velocities by approximately 2% at typical mantle adiabatic conditions. This gives an indication of the uncertainties in current seismic velocity estimates; to put this into context, this is the same variation in velocities that would arise from temperature differences of approximately 800 K. If measurements could be made at mantle temperatures, however, the need for thermal extrapolation of the measured velocities would be removed, so that the uncertainties that need to be taken into account are those arising only from the measurements themselves, which are typically near 0.5%.

The ability to perform elasticity measurements at mantle temperatures and pressures is an important challenge, but it is beset by difficulties. For ultrasonic experiments in the multi-anvil apparatus, high temperatures invariably cause problems due to sample grain growth, preferred orientation and plastic deformation, with the latter likely to lead to uncertainties in sample length determination. Brillouin measurements on single crystals in the DAC have been performed using resistive heaters placed around the diamonds. Temperatures are generally limited to below 1200 K (Lu et al. 2013; Pamato et al. 2016), however, due to the long heating times required for the scattering measurements and the potential for the diamonds and DAC body to be oxidized. One promising methodology is the use of a graphite resistive heater in combination with a vacuum chamber to minimize DAC oxidation (Immoor et al. 2020), which was recently used to obtain temperatures of nearly 2000 K. However, such a heater requires a water-cooled vacuum chamber to prevent the oxidation not only of the DAC elements but especially of the heater itself, therefore such a setup cannot be easily coupled with a Brillouin system. Mantle temperatures can potentially also be reached through the use of laser heating in the DAC. This is challenging since the transparent samples employed cannot be heated by conventional near-infrared (NIR) laser heating systems, but require the use of a CO_2 laser (Murakami et al. 2009, 2012; Zhang et al. 2015; Zhang and Bass 2016). There is, however, a major advantage related to the use of such a laser, because its wavelength of 10.6 µm ensures homogeneous heating of relatively thick (15–20 µm) silicate materials, regardless of the presence of NIR-absorbing species (e.g., iron). This is achieved thanks to the different laser absorption mechanism of the CO_2 laser with respect to the NIR laser. In fact, the NIR laser radiation, typically used for heating metallic materials, is absorbed primarily at the surface of the sample, creating large gradients inside the sample, which can be reduced only by heating both sides of the sample (see Anzellini and Boccato 2020 for a review). Instead, the CO_2 radiation is absorbed by the lattice vibrations of the material, ensuring uniform heating throughout the entire thickness of the sample, with negligible axial thermal gradients, so that it is not necessary to construct a heating system that heats from both sides (Anzellini and Boccato 2020). Unfortunately, because of its long wavelength, not only the direct beam, but also the diffuse radiation is extremely dangerous for the human skin. At the Bayerisches Geoinstitut (BGI), we have developed a system in which the laser beam is completely enclosed right up to the diamond anvil cell either using a flexible optical hollow silica waveguide (Kurnosov et al. 2019) or an articulated arm. Brillouin scattering data of single crystals of pyrope have been measured up to pressures of 23.8(1) GPa and at temperatures between 850 and 1900 K with a three-fold objective: (i) to characterize the advantages and disadvantages of the two different enclosure techniques; (ii) to benchmark the CO_2 laser system with an extensively studied material at high P and T, to evaluate the accuracy and precision of the method before measurements on completely unknown materials are performed; (iii) to provide strong constraints on the elastic behaviour of pyrope that allow interpretation of seismic profiles using mineral-physics models.

Methods

Sample preparation

Several single crystals of pyrope (space group $Ia\bar{3}d$) with dimensions between 100 and 150 µm were selected from a natural sample from the Dora Maira Massif (Italy) with composition $Mg_{2.96}Fe_{0.05}Al_{2.04}Si_{2.95}O_{12}$ (Aubaud et al. 2007). This sample has been well characterized in terms of purity and microstructure (Chopin 1984) and contains a negligible amount of water (44 ppm) (Aubaud et al. 2007). The selected crystals were inclusion free and revealed sharp diffraction profiles in omega scans (full width at half maximum < 0.08°) obtained using a Huber four-circle diffractometer in combination with a FR-E + SuperBright microfocus rotating anode X-ray source employing Mo Kα radiation (Trots et al. 2011) and a point detector, driven by the program SINGLE (Angel and Finger 2011). The unit-cell volume of this pyrope was determined at room

conditions by measuring 22 reflections centered with the 8-positions method (King and Finger 1979). The unit-cell axis and volume of pyrope, refined using the vector least-squares method (Ralph and Finger 1982) are the following: $a = 11.45560(13)$ Å and $V = 1503.33(5)$ Å^3, resulting in a density of 3.572 g/cm^3. The selected pyrope crystals were double-side polished in random orientations down to a thickness of 18 µm and cut using a FEI Scios focused ion beam into optically transparent disks of approximately 60–70 µm in diameter. One to three of these cylinders were loaded between two thin layers of KBr (for measurements at pressures below 8 GPa) or KCl (for measurements at pressures above 8 GPa) in a pressure chamber of a BX-90 DAC (Kantor et al. 2012) with a 90° optical opening angle. Both KBr and KCl provide sufficient thermal insulation of the sample from the heat-conductive diamond anvils and are relatively soft pressure transmitting media especially at high temperature. The need to use two different isolating materials arises from the fact that the Brillouin signals of the soft pressure transmitting media are more sensitive to pressure than those of pyrope. For instance, at 8 GPa the v_S of pyrope starts to overlap with the v_P of KBr, whereas above this pressure there is no more overlap between the pyrope v_S and the KCl v_P. A ruby chip and a crystal of Sm-doped $Y_3Al_5O_{12}$ garnet (Sm: YAG), both used as pressure calibrants, were placed between one of the diamond anvil surfaces and the KBr/KCl layers.

CO2 laser heating system

Two different technologies, developed mainly for medical surgeries, were used to guide the CO_2 laser within a completely enclosed environment. The first, shown in Fig. 1, makes use of a flexible hollow silica waveguide (HSW) described in detail by Kurnosov et al. (2019) and the second uses an articulated arm (AA), model S-7 from CNI Laser (China), with seven junctions in which mirrors are mounted to direct the laser to the exit point (Fig. 2). Either the HSW or the AA were used to guide the light produced by a fan-cooled 100 W Synrad Firestar CO_2 laser to the DAC used for the Brillouin scattering measurements, which was mounted on a 4-circle Huber goniometer. The end of the HSW is inserted into an optical cage system from Thorlabs (Fig. 1), mounted on top of an XYZ stage and a magnetic mount and equipped with two 25.4 mm diameter ZnSe lenses, one with a 200 mm focal length and the other with 50 mm, which are used to collimate and focus, respectively, the CO_2 laser beam onto the sample (Kurnosov et al. 2019). This system was used for measurements up to ~12 GPa.

The AA, on the other hand, has a 50 mm focal distance lens incorporated at the final junction. To achieve the desired focusing, this junction is mounted on a XYZ translation stage (Fig. 2). This setup was used for measurements up to 23 GPa.

In both cases the laser is focused on the sample inside the DAC by monitoring the power exiting the pressure chamber using a power-meter installed on the detector arm of the 4-circle Huber diffractometer behind the DAC. The sample is continually monitored using a Mitutoyo x5 long working distance objective mounted on a separate XYZ stage, combined with a CCD camera.

In situ pressure determination

Typically, during laser heating experiments, pressure is determined at room temperature before and after the

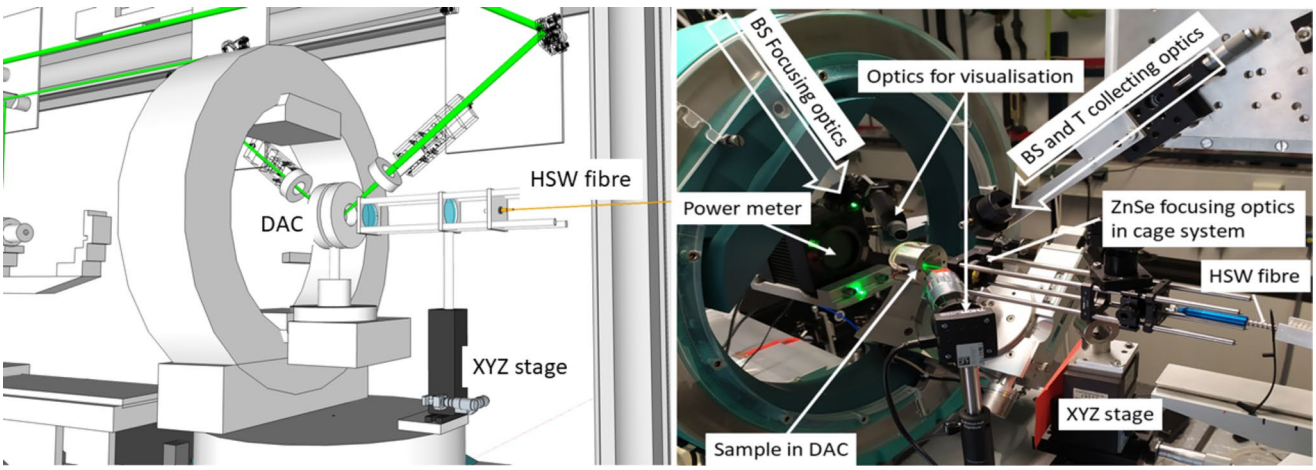

Fig. 1 Schematic drawing (left) of the hollow laser waveguide mounted on a XYZ stage equipped with two ZnSe lenses for collimating and focusing the CO_2 laser beam into the sample inside the DAC. A photograph (right) of the system build onto the Huber goniometer, including the optic camera for visualization and power meter for monitoring the laser power exiting the pressure chamber that facilitates focusing of the CO_2 laser beam on the sample. For reference, the diameter of the diamond anvil cell used is 50 mm. BS stands for Brillouin scattering and T is temperature

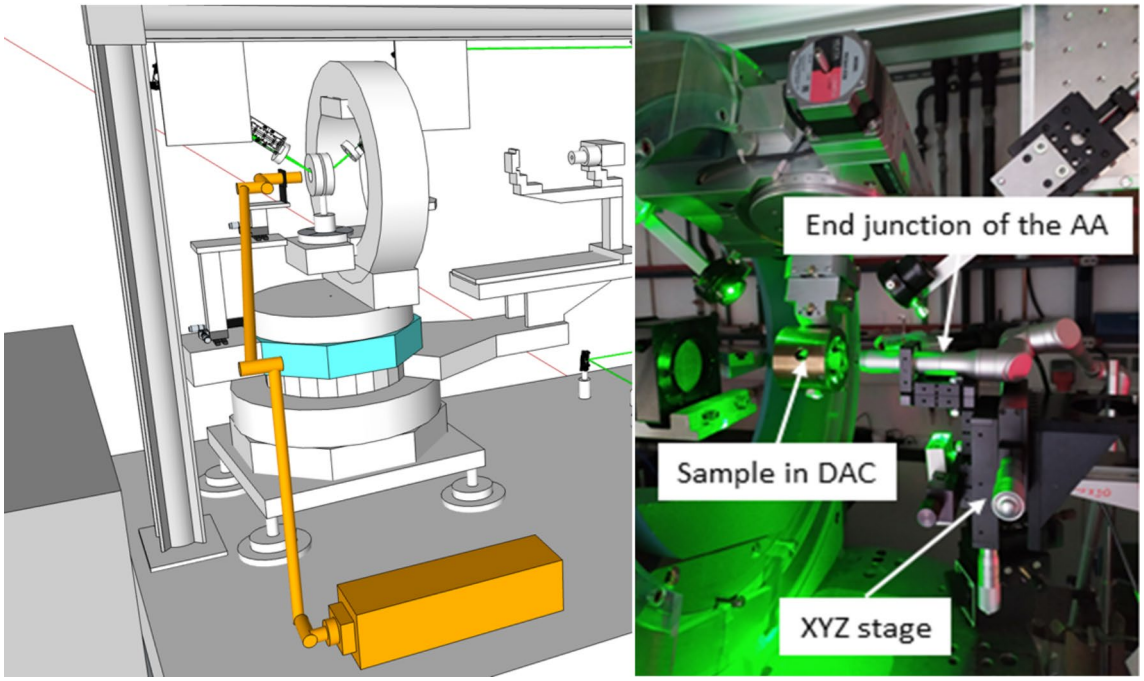

Fig. 2 Schematic drawing (left) of the articulated arm attached to the CO_2 laser (in orange) on the optic table of the Brillouin + XRD system; and picture (right) of the end junction mounted onto a XYZ stage directly in front of the DAC. Power-meter and optics for visualization are the same as used for the HSW system (Fig. 1). The diamond anvil cell used with the AA is inserted into a membrane cylinder of 60 mm diameter

laser-heating cycles using the ruby luminescence and the pressure at temperature is assumed to be an average between the two pressure measurements. A number of studies, however, have shown that the effect of thermal pressure due to laser heating is significant (Andrault et al. 1998; Dewaele et al. 1998; Andrault and Fiquet 2001). Depending on the strength of the sample and of the pressure transmitting medium, the thermal pressure can be localized in the hot spot or equilibrated within the sample chamber. In this work, the whole sample is heated by the laser spot, moreover the pressure gradients in the highly compressible KBr or KCl material are likely small at the temperatures reached in this study, therefore the thermal pressure during laser heating is expected to be equilibrated during the time scale of the Brillouin measurements. In order to monitor the changes in pressure due to laser heating we use Sm-doped $Y_3Al_5O_{12}$ garnet, Sm: YAG, since the change with pressure of its Y1 and Y2 luminescence lines have been calibrated (Trots et al. 2013) and are temperature independent, contrary to the luminescence lines of ruby, at least up to 850 K (Hess and Schiferl 1992; Goncharov et al. 2005). Sm: YAG luminescence spectra (i.e. Fig. 3 left) were collected using a Princeton Instruments "Acton" Raman Spectrometer with a PIXIS camera. An 1800 g/mm grating was used for high resolution measurements of the luminescence peaks. The luminescence signal is delivered to the spectrometer through the same optical pathway used for the Brillouin measurements by inserting a mirror and a focusing lens behind the pinhole to direct the laser into the Raman spectrometer. Pressure based on the frequency shift of the Y1 line of Sm: YAG is indeed found to increase by at least 0.5 (1) GPa during heating due to thermal expansion in the sample chamber but remains constant for a given laser heating power. Because Sm: YAG is in contact with the diamond and the DAC is inserted into a massive stainless-steel cylinder flushed with compressed air, we expect a minimal temperature increase (less than 100 °C) recorded by Sm: YAG, i.e. well below the temperature that would affect its luminescence lines.

In situ temperature measurements

To determine temperature, three to five thermal radiation spectra (i.e. Fig. 3 right) were collected during laser heating before and after the Brillouin scattering measurements using a Princeton Instruments "Acton" Spectrometer with a PIXIS camera and 150 g/mm wide-range grating. The temperature values from all collected spectra at a given pressure point were averaged and the standard deviation was used as a *T* uncertainty. The thermal radiation spectra were recorded through the Brillouin optical system by using a pinhole at the entrance of the Fabry–Pérot Brillouin interferometer to analyze an image that corresponds to a 40 µm diameter spot on the sample platelet. In this way the sample thermal radiation and the Brillouin scattering measurement are collected

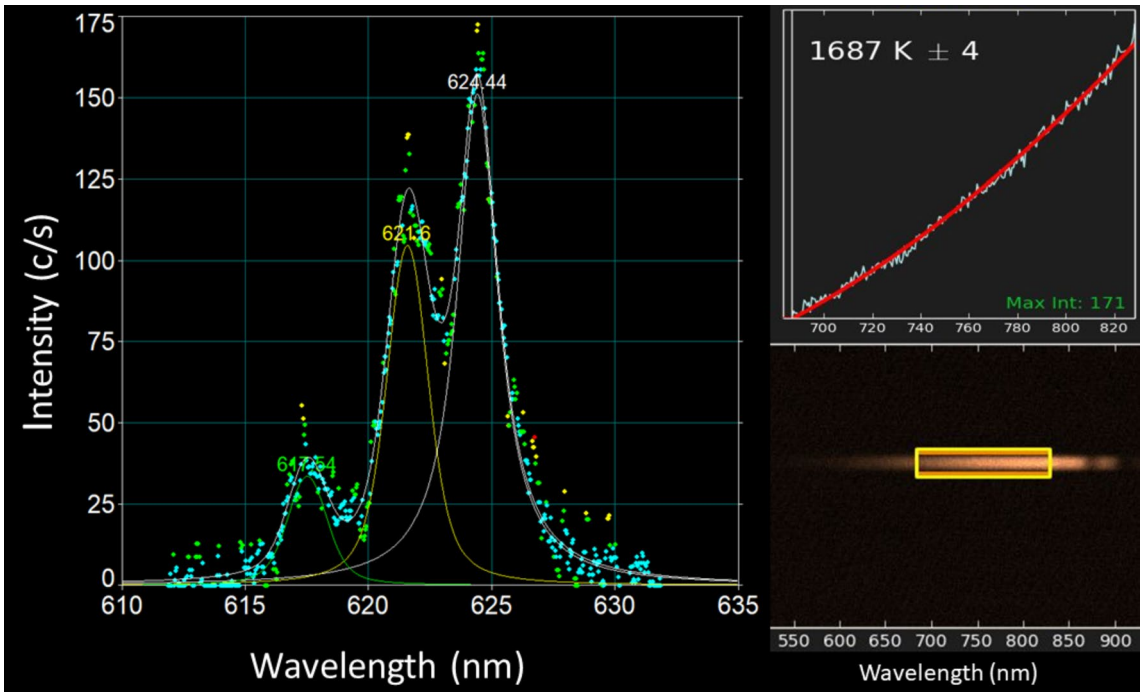

Fig. 3 (left) Sm: YAG luminescence spectrum collected using the LightField software during laser heating at $P = 18.8$ GPa and analyzed with the PeakFit software and (right) the thermal radiation spectrum collected at the same pressure of the laser heated pyrope crystal using the LightField software and analyzed with T-Rax software provided by C. Prescher

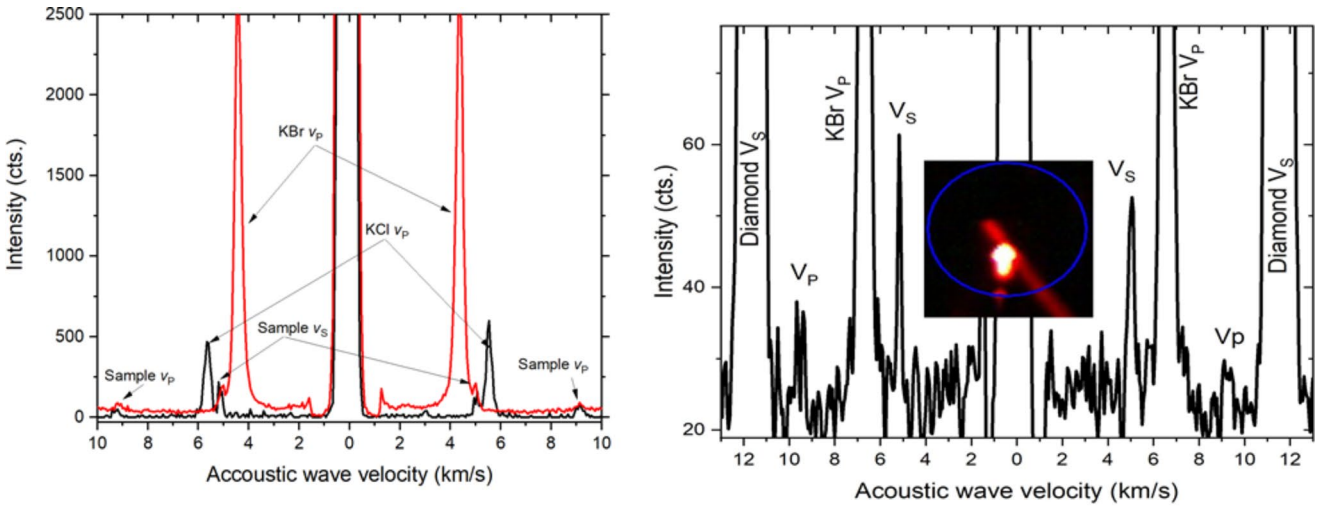

Fig. 4 (left) Comparison between a Brillouin spectrum collected at 8.3 GPa and room temperature (red) in KBr, at a pressure just before the v_S peak of the sample overlaps with the v_P peak of the pressure medium and a Brillouin spectrum collected at 8.5 GPa and room temperature (black) in KCl, just after the pressure at which the v_S peak of the sample overlaps with the v_P peak of the pressure medium; (right) Brillouin spectrum collected at 20 GPa and 1900 K. An image of the pyrope crystal while being heated with the CO_2 laser using the articulated arm is shown in the inset

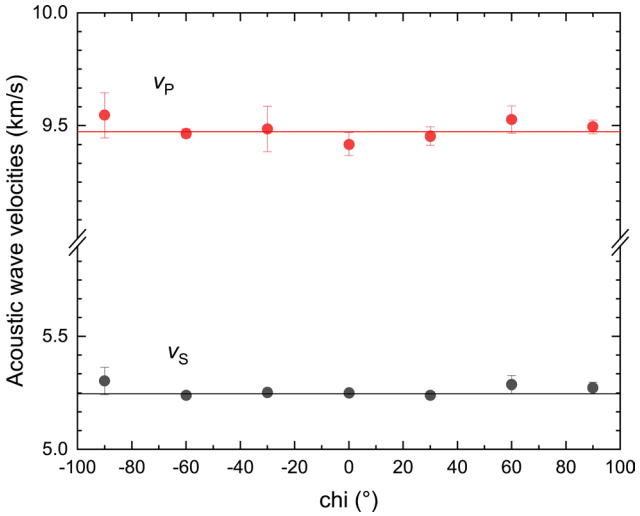

Fig. 5 Acoustic wave velocities of pyrope at 6.39 GPa and room temperature after heating up to 1677 (50) K, collected at different orientations obtained by rotating the chi diffractometer circle, showing the negligible anisotropy of the garnet structure

from exactly the same area of the sample, and the insertion of a mirror behind the entrance pinhole is used to switch easily between the Brillouin scattering measurements and temperature measurements. This approach reduces temperature uncertainties that may otherwise arise from misalignments. The thermal radiation spectra were analyzed using the T-Rax software (by C. Prescher), applying a temperature calibration performed using a pre-calibrated tungsten-lamp.

Brillouin scattering measurements at simultaneous high-pressures and high-temperatures

Brillouin scattering measurements were performed using the system installed at the Bayerisches Geoinstitut (Trots et al. 2013). This system employs a Coherent Verdi V2 solid-state Nd: YVO_4 laser with a 532 nm single wavelength output, a six-pass Sandercock-type piezoelectrically driven scanning tandem Fabry-Pérot interferometer (Sandercock 1982) and a single pixel photon counter detector (Hamamatsu C11202-50). The incident laser beam is focused onto the sample and the scattered light is collected from the sample through optical paths consisting of sets of lenses and mirrors with motorized adjustments along the optical axis of the DAC. The distance between the sample and the collecting lens is 100 mm, whereas that between the focusing lens and the entrance pinhole of the Brillouin spectrometer is 500 mm. This provides a magnification factor of 5:1. A 200 µm pinhole size was used for all measurements, this ensures that the analyzed sample area is 40 µm, i.e. smaller than the CO_2 laser hotspot size. A laser power of 400 mW was used to collect the Brillouin spectra. The scattering angle between the incident laser beam and the analyzed scattered light was regularly controlled and calibrated using a fused silica glass standard. All Brillouin scattering experiments were conducted in a symmetric platelet geometry (Speziale et al. 2014; Whitfield et al. 1976).

Brillouin spectra at high pressure and room temperature were collected after annealing at high temperature for up to 2 h. Pyrope samples were measured in different crystal directions in order to examine the effect of different pressure media on the room temperature elasticity of pyrope. Probing different directions was important in this case because any deviation from the practically isotropic behaviour, which has been reported for cubic garnets both at room conditions and at high-pressures and temperatures (Sinogeikin and Bass 2000, 2002; Lu et al. 2013; Pamato et al. 2016), would suggest a possible tilt of the crystal (i.e. a deviation from the platelet geometry) or alteration of the crystal due to the heating cycles.

Given the negligible anisotropy of pyrope, however, Brillouin spectra at high temperature were collected only in one direction in order to reduce the number of measurements and in this way to minimize the degradation of the sample surface at high-temperature. During these measurements the diamond anvil cell was cooled using a flux of compressed air. Increasing temperature increases thermal fluctuations in the sample and, therefore, the number of photon-phonon scattering events. This allows for faster data collection, so that at high temperatures a reasonable signal to noise ratio for the Brillouin signal was obtained after collection times of between two to ten minutes, versus approximately 30 min at room temperature for a comparable signal strength.

Several loadings were necessary to cover the pressure-temperature range of this study, due to the degradation of the crystal surfaces as a result of the prolonged laser heating. After each temperature cycle, if the crystals were not damaged, pressure was increased manually after removing the DAC from the X-ray diffractometer. After every pressure increase or new loading, the sample in the DAC was carefully aligned into the centre of rotation of the Eulerian cradle and care was taken to preserve the symmetric platelet geometry.

The Brillouin signals were analyzed using the program Brillouin Win1024 version 2.6.3 written by S. Sinogeikin and the signal to noise ratio of the Brillouin peaks was used to estimate the uncertainties in wave velocity values (Pamato et al. 2016). Brillouin scattering spectra have been collected at several temperatures up to 1923 K and at different pressures up to 23.8 GPa. A comparison between Brillouin spectra collected in KBr and KCl at room temperature and 8.3 and 8.5 GPa respectively as well as an example of a Brillouin spectrum collected at high temperature are shown in Fig. 4. Both acoustic wave velocities, v_P and v_S, of pyrope

are clearly visible together with the signals of the pressure transmitting media.

Results

Comparison between the two laser beam delivery systems

In this study two different types of CO_2 laser beam delivery systems were tested; the first uses a flexible HSW and the second one uses a series of mirrors housed at the junctions of an AA. The flexible HSW system provides the possibility of guiding the laser to a distance of up to 3 m from the laser source. However, the internal reflective layer of the waveguide is damaged significantly for integral laser powers above 20 W, limiting, therefore, the system to use at lower pressures, where the sample can be easily insulated from the diamonds and can, therefore, be heated using such lower laser power. For example, in this study we could reach ~ 1650 K at 11.6 GPa with the HSW, but could not increase the temperature further because the integral power of the CO_2 laser was already 20 W. With this limited power we were unable to heat the pyrope samples at pressures higher than 12 GPa.

The AA used in this work requires the CO_2 laser to be mounted within one meter from the four-circle diffractometer, but it provides stable transmission of the CO_2 laser beam up to an integral power of 60 W. Short laser beam transmissions (max 10 min) were tested using the full laser power of 100 W, however for longer operation times needed for collecting Brillouin spectra with good signal to noise ratio (i.e. more than 30 min of constant transmission) overheating of the junctions and consequent damage of one of the mirrors occurred at integral laser power above 60 W. In the present study a maximum integral laser power of only 40 W was needed to reach 1790 (67) K at 23.7 GPa. Note that the AA used in this study is equipped with gold coated quartz-based mirrors without external cooling. Using an AA with metallic mirrors would likely increase the maximum laser power, which can be sustained without failure of the mirrors even without external cooling.

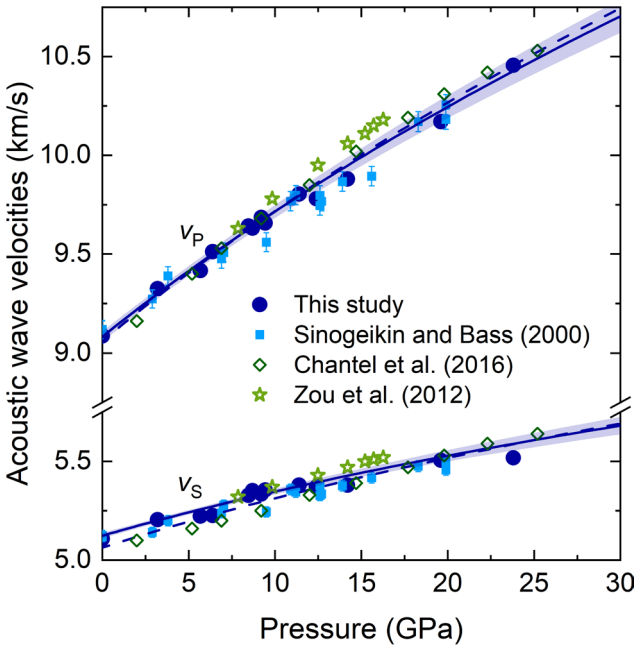

Fig. 6 Variation with pressure of the acoustic wave velocities of pyrope at room temperature. The solid curve shows the pressure dependence of v_P and v_S wave velocities determined using the EoS parameters obtained in this study (the shaded areas indicate the propagated uncertainties of the EoS parameters). The dashed curve shows the global fit EoS from Chantel et al. (2016)

High pressure and room temperature elasticity of pyrope

The acoustic wave velocities of pyrope were measured as a function of pressure at room temperature after each high-temperature annealing. Measurements were also made in several different crystal orientations and an example of a dispersion curve collected at 6.39 GPa, after high-temperature measurements up to 1677(50) K is shown in Fig. 5. The standard deviations of the average of the v_S and v_P values are 24 m/s and 43 m/s, respectively and reflect the 1σ uncertainties of the individual velocities, confirming that the anisotropy of pyrope is negligible, as reported in previous studies (Sinogeikin and Bass 2000, 2002). As shown in Fig. 6 the room temperature velocities (i.e. the average of the values collected in different directions) are in very good agreement with those obtained for a single-crystal of synthetic pyrope using Brillouin scattering by Sinogeikin and Bass (2000). In fact, the extent of scattering, particularly in v_P, is smaller in the current study. Sinogeikin and Bass (2000) used a 16:3:1 by volume mixture of methanol–ethanol–water as a pressure transmitting medium in their experiments. Above 10 GPa, however, they externally heated the DAC to relax non-hydrostatic stresses before each measurement, which were assessed by measuring pressure gradients using ruby-luminescence. The very good agreement between the two studies indicates that laser heating also relaxes non-hydrostatic stresses that might accumulate on the crystal at room temperature due to the use of KBr and KCl as pressure transmitting media. Given the good agreement, we can also conclude that the small amount of Fe present in the natural pyrope used in this study (Fe/[Fe + Mg] = 0.017) has a negligible effect on the wave velocities of the pyrope end-member. This is expected given the small difference in the molar volume between the natural sample used in this study

Table 1 Acoustic velocities collected at high-pressures and high-temperatures for pyrope

P (GPa) *	T (K)	v_S (km/s)	v_P (km/s)	ρ (g/cm^3)
Run 1 (HSW fiber)				
0.0001	298 (1)	5.108 (31)	9.087 (40)	3.573 (5)
3.20	298 (1)	5.205 (26)	9.325 (30)	3.639 (5)
3.29	1358 (50)	5.028 (30)	9.120 (48)	3.507 (5)
3.32	1413 (62)	5.080 (24)	9.112 (37)	3.500 (5)
3.38	1413 (61)	5.041 (38)	9.109 (66)	3.501 (5)
3.30	1487 (50)	5.028 (28)	9.142 (33)	3.489 (5)
3.35	1490 (50)	5.035 (26)	9.075 (30)	3.490 (5)
3.31	1500 (94)	4.954 (38)	9.000 (79)	3.487 (5)
3.31	1598 (77)	5.050 (58)	9.023 (79)	3.474 (5)
5.68	298 (1)	5.223 (16)	9.416 (19)	3.688 (5)
5.69	851 (50)	5.191 (30)	9.339 (48)	3.625 (5)
5.75	934 (50)	5.195 (38)	9.375 (45)	3.616 (5)
5.73	972 (188)	5.171 (26)	9.299 (38)	3.610 (5)
5.68	1486 (50)	5.094 (30)	9.275 (38)	3.541 (5)
5.73	1182 (68)	5.177 (28)	9.320 (43)	3.583 (5)
5.72	1214 (115)	5.126 (30)	9.312 (48)	3.578 (5)
5.75	1287 (64)	5.107 (30)	9.237 (38)	3.569 (5)
5.75	1318 (50)	5.077 (30)	9.258 (58)	3.565 (5)
5.82	1414 (67)	5.068 (37)	9.209 (48)	3.554 (5)
5.82	1418 (90)	5.090 (26)	9.231 (33)	3.553 (5)
5.84	1419 (50)	5.095 (30)	9.213 (66)	3.554 (5)
5.82	1453 (97)	5.070 (26)	9.236 (38)	3.548 (5)
5.92	1525 (68)	5.065 (30)	9.204 (38)	3.541 (5)
6.39	298 (1)	5.226 (33)	9.512 (48)	3.702 (5)
6.78	1100 (114)	5.159 (26)	9.384 (58)	3.615 (5)
6.87	1194 (50)	5.132 (26)	9.353 (43)	3.605 (5)
6.92	1296 (50)	5.159 (30)	9.399 (48)	3.592 (5)
6.78	1324 (50)	5.107 (30)	9.346 (48)	3.586 (5)
6.82	1395 (50)	5.090 (30)	9.353 (48)	3.577 (5)
6.94	1425 (50)	5.103 (26)	9.344 (48)	3.576 (5)
6.88	1626 (50)	5.074 (26)	9.294 (48)	3.548 (5)
6.92	1677 (50)	5.076 (48)	9.195 (58)	3.542 (5)
7.56	1203 (157)	5.173 (48)	9.448 (48)	3.618 (5)
7.50	1501 (63)	5.129 (38)	9.381 (43)	3.577 (5)
8.47	298 (1)	5.328 (24)	9.642 (38)	3.741 (5)
8.70	298 (1)	5.352 (26)	9.631 (43)	3.745 (5)
8.87	1392 (122)	5.214 (33)	9.508 (43)	3.619 (5)
8.50	1440 (50)	5.220 (20)	9.479 (37)	3.606 (5)
8.87	1445 (62)	5.192 (33)	9.474 (43)	3.612 (5)
8.88	1487 (103)	5.229 (38)	9.464 (48)	3.607 (5)
8.83	1923 (85)	5.116 (38)	9.423 (58)	3.549 (5)
9.20	298 (1)	5.335 (30)	9.685 (38)	3.754 (5)
9.43	298 (1)	5.355 (20)	9.657 (26)	3.758 (5)
9.46	1308 (117)	5.234 (24)	9.554 (30)	3.642 (5)
9.57	1329 (58)	5.278 (22)	9.586 (26)	3.641 (5)
9.52	1454 (142)	5.218 (24)	9.540 (30)	3.624 (5)
9.52	1513 (68)	5.246 (26)	9.508 (33)	3.617 (5)
11.40	298 (1)	5.380 (18)	9.804 (22)	3.794 (5)
11.86	974 (117)	5.295 (26)	9.682 (26)	3.729 (5)
11.86	1124 (116)	5.273 (24)	9.677 (33)	3.711 (5)
11.53	1161 (81)	5.254 (22)	9.641 (30)	3.700 (5)
11.23	1190 (150)	5.286 (30)	9.682 (38)	3.691 (5)
11.86	1378 (189)	5.271 (26)	9.667 (38)	3.679 (5)
11.53	1480 (69)	5.256 (30)	9.664 (30)	3.660 (5)

Table 1 (continued)

P (GPa) *	T (K)	v_S (km/s)	v_P (km/s)	ρ (g/cm^3)
11.63	1663 (50)	5.268 (26)	9.643 (38)	3.639 (5)
Run 2 (AA)				
19.68	298 (1)	5.506 (40)	10.170 (40)	3.930 (5)
19.68	1577 (88)	5.352 (20)	10.059 (50)	3.789 (5)
19.68	1615 (49)	5.368 (30)	10.035 (50)	3.776 (5)
19.60	1744 (67)	5.344 (20)	10.009 (30)	3.767 (5)
19.7	1761 (82)	5.387 (30)	9.996 (70)	3.759 (5)
19.68	1412 (28)	5.435 (20)	10.021 (70)	3.806 (5)
23.96	1790 (67)	5.386 (30)	10.202 (70)	3.841 (5)
23.69	1709 (97)	5.426 (30)	10.294 (70)	3.865 (5)
23.96	298 (1)	5.518 (30)	10.456 (50)	3.995 (5)

*Note: the uncertainties on pressure are smaller than 0.08 GPa

(113.16 cm^3/mol) and the pyrope end-member (113.13 cm^3/mol as reported by Angel et al. 2022).

The two most extensive ultrasonic measurements of polycrystalline pyrope samples measured using a multi-anvil apparatus (Chantel et al. 2016; Zou et al. 2012) are also reported in Fig. 6 for comparison. A detailed comparison among ultrasonic wave velocity data including Gwanmesia et al. (2006, 2007) and Chen et al. (1999) is given in Chantel et al. (2016). The room temperature wave velocities determined in the current study are in reasonable agreement with the ultrasonic measurements of Chantel et al. (2016), although there is a clear difference in slope with pressure that is most evident in v_S at pressures below 15 GPa. The lower values of v_S at lower pressures may result from microporosity within the hot-pressed samples, that might only close at higher pressures due to the relatively high strength of pyrope (Li et al. 2006). Higher values of both v_S and v_P at higher pressures in the ultrasonic study of Chantel et al. (2016) might result from the development of high levels of deviatoric stress in the samples during room temperature compression. The aggregate velocities of pyrope measured ultrasonically by Zou et al. (2012) are higher, compared to the other studies, at pressures above 10 GPa (Fig. 6). Each room temperature measurement, in this previous study, was made after high temperature annealing, which should, therefore, have relaxed any non-hydrostatic stresses. The origin of this difference, which increases systematically with pressure, is therefore hard to evaluate.

P-V-T-v_S-v_P equation of state of pyrope

Given the negligible anisotropy of pyrope over the pressures and temperatures of its stability, the acoustic wave velocities measured in any direction at a given *P* and *T* can be considered to be representative of the aggregate wave velocity of pyrope, i.e.

$v_P = \sqrt{\frac{K_S + {}^4/_3 G}{\rho}}$ and $v_S = \sqrt{\frac{G}{\rho}}$, where K_S is the adiabatic bulk modulus, G is the shear modulus and ρ is the density at any given condition. As such all 64 acoustic wave velocity measurements collected in this study (Table 1) were used directly in a fitting routine implemented in the Origin software (Buchen 2018), which makes use of a self-consistent thermodynamic formalism employing a modified Mie-Grüneisen equation of state with a Debye approximation, according to the equations based on the Eulerian strain reported by Stixrude and Lithgow-Bertelloni (2005). Because the Mie-Grüneisen equation of state is expressed in terms of isothermal parameters, whereas elastic wave propagation is an adiabatic process, the adiabatic bulk moduli are converted to isothermal values, K_T, during each step of the fitting procedure using the relationship:

$$K_S = K_T + \frac{TC_V\gamma^2}{V} \quad (1)$$

where V is the volume in cm^3/mol, T the temperature in Kelvin, C_V the heat capacity at constant volume in kJ/(mol K) and γ the Grüneisen parameter. In this formalism C_V is expressed in terms of the Debye temperature θ:

$$C_v = 9nR\left(\frac{T}{\theta}\right)^3 \int_0^{\theta/T} \frac{e^t t^4}{(e^t-1)^2} dt \quad (2)$$

with n the number of atoms in the formula unit of pyrope and R the gas constant in J/(mol K). The room pressure density, ρ_0, is fixed to the value determined in this study, whereas densities at high pressures and temperatures are obtained through an iterative procedure, starting from the values determined using the equation of state parameters reported by Angel et al. (2022) at the pressures measured using Sm: YAG. In this procedure, the analytical approximation of the Debye function proposed by Anderson (2019) was employed. Initially, the room pressure bulk and shear moduli, K_{T0} and G_0, their first pressure derivatives, K_{T0}' and G_0', the Grüneisen parameter γ_0 and its

Table 2 Thermo-elastic parameters of pyrope

	K_{T0} (GPa)	K'_{T0}	G_0 (GPa)	G'_0	γ_0	q	θ_0 (K)	η_0
This study	168.2 (1.5)	4.30 (20)	93.8 (5)	1.48 (6)	1.22 (14)	0.03 (35)	823*	0.21 (10)
Chantel et al. (2016) global fit	169.5 (2.6)	4.38 (20)	91.4 (6)	1.55 (10)	1.15 (30)	1.5*	823*	0.45 (30)
Angel et al. (2022)	169.4 (3.0)	4.55 (5)	==	==	1.185 (12)	0.79 (17)	771 (28)	==
Stixrude and Lithgow-Bertelloni (2024)	170.0 (2.0)	4.10 (30)	94.0 (2)	1.40 (2)	1.010 (6)	1.4 (5)	843 (4)	1.00 (3)

* fixed values

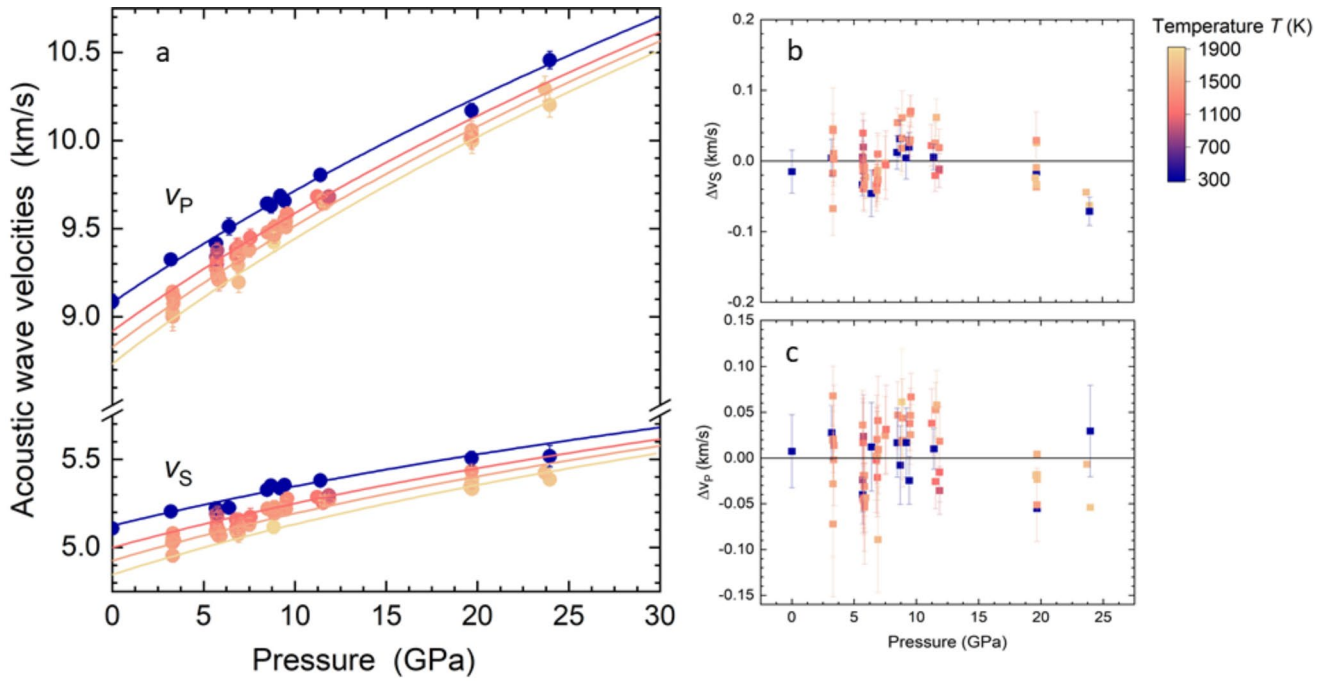

Fig. 7 Variation with pressure of **a**) the acoustic wave velocities of pyrope measured in this study (filled circles) at different temperatures (colour coded). Solid curves have been calculated at 298, 1000, 1500 and 1900 K using the EoS parameters resulting from the *P-T*-finite strain fitting procedure; and **b**, **c**) the difference between calculated and observed acoustic wave velocities v_S and v_P respectively showing that the agreement is better than 100 m/s at all temperatures

shear strain derivative η_{S0} and the parameter q_0, were all fitted, whereas the room pressure Debye temperature, θ_0, was fixed to the value of 823 K, as in the study of Chantel et al. (2016). Results of this initial fitting highlighted the strong correlation between γ_0 and η_{S0} with a correlation coefficient of -0.97, for this reason in the following cycles the two parameters were not refined simultaneously. A range of fitting parameters were found that could suitably fit the entire data set from this study, and were in good general agreement with the other pyrope elasticity studies. However, only a sub-set of these fitting parameters could reproduce the ambient pressure thermal expansion data on pyrope (Milani et al. 2015). In a second round of optimization the elasticity data set from our study were, therefore, fitted using the volume-temperature measurements of Milani et al. (2015) as a further constraint. The resulting fit parameters are reported in Table 2, where they are compared with previous assessments. A comparison between the EoS fits and the velocity data measured in this study is shown in Fig. 7. The difference between calculated and observed acoustic wave velocities is below 100 m/s at all temperatures, with the majority of data actually deviating by less than 50 m/s, particularly for v_S.

A comparison between the volume of pyrope at ambient pressure and high temperature calculated using the EoS parameters determined in this study and the volume data measured in previous studies is shown in Fig. 8. Overall the model is in good agreement with a range of volume data recently measured at ambient pressure for pyrope. The parameters reported by Stixrude and Lithgow-Bertelloni (2024), instead, result in a smaller variation with temperature of the unit-cell volume of pyrope more in agreement with the older study of Skinner et al. (1956).

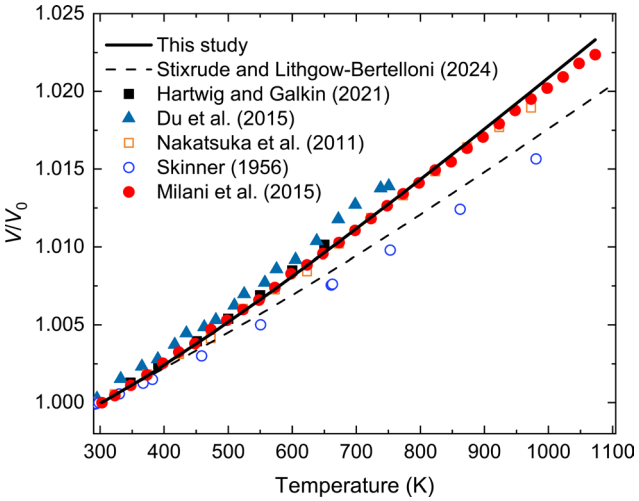

Fig. 8 Variation with temperature of the unit-cell volumes of pyrope measured in previous studies normalised with respect to the corresponding room temperature values, compared with the high-temperature variations obtained from the EoS parameters determined in this study (solid curve) and those reported in Stixrude and Lithgow-Bertelloni (2024) (dashed curve)

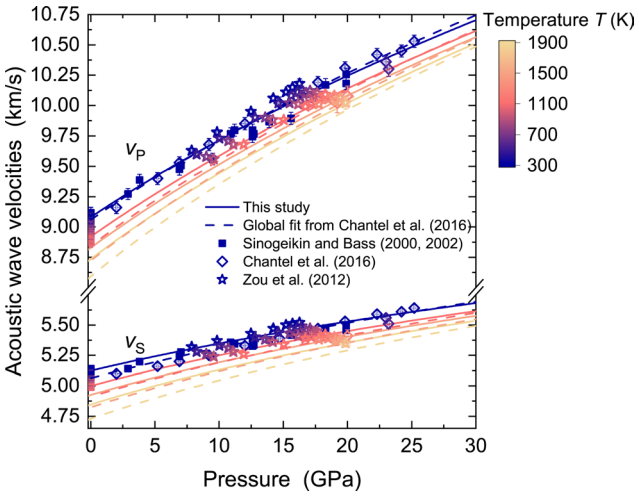

Fig. 9 Variation with pressure of the acoustic wave velocities of pyrope determined in previous studies at different temperatures indicated by the colour scheme, compared with isotherms calculated at 300, 1100, 1500 and 1900 K obtained using the EoS parameter determined in this study (solid lines) and the global fit EoS parameters (dashed lines) reported by Chantel et al. (2016). For the values determined in this study see Fig. 7

Discussion

In Fig. 9 isothermal curves calculated using the pyrope EoS parameters determined in this study (Table 2) and also using the global fit parameters reported by Chantel et al. (2016), are compared with wave velocities measured in previous studies using Brillouin scattering (Sinogeikin and Bass 2000, 2002) and ultrasonic techniques (Chantel et al. 2016; Zou et al. 2012). The isotherms calculated using our EoS are

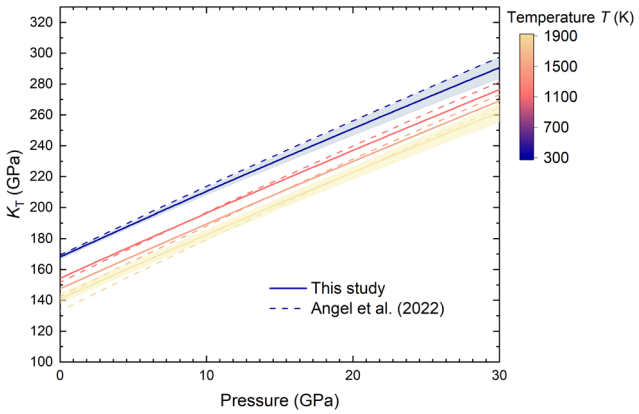

Fig. 10 Variation with pressure of the isothermal bulk modulus of pyrope calculated at 300, 1100, 1500 and 1900 K (color scheme) using the EoS parameters obtained in this study and those obtained by Angel et al. (2022). The shaded areas represent the propagated uncertainties for K_T at room temperature and at 1900 K

in general agreement with previous measurements and the differences, particularly with the data of Zou et al. (2012), decrease with increasing temperature. As can be seen in Fig. 9, except for the ambient pressure measurements of Sinogeikin and Bass (2002), which only extend to 1073 K, there is a lack of lower pressure, high-temperature data in previous studies.

By comparison with Fig. 7, it can be seen that in the current study there are more constraints on velocities at mantle-temperatures both below and above 10 GPa. The deviation between our EoS model and the previous global fit model proposed by Chantel et al. (2016), which was based on a fit to all the experimental data shown in Fig. 9, is the greatest at the conditions where the previous data coverage was the poorest. At high pressures the isotherms calculated in this study tend to converge with those of Chantel et al. (2016) but there is still a degree of divergence once temperatures become higher than 1100 K. It seems, therefore, that our EoS is in good agreement with previous high-temperature measurements, which, provides an important benchmark for the laser heated technique. However, a global fit to these previous data (Chantel et al. 2016) does not extrapolate optimally to reproduce the higher temperature velocities measured in our study.

A further comparison can be made between our EoS and the *P-V-T* EoS recently refined by Angel et al. (2022) using a combination of compressibility, thermal expansion, elasticity and heat capacity data for pyrope. The Mie-Grüneisen-Debye EoS used by Angel et al. (2022) is practically equivalent to the finite strain expressions used in this study (Stixrude and Lithgow-Bertelloni 2005), as demonstrated by Criniti et al. (2024). In Fig. 10 the variation with pressure of the isothermal bulk modulus (K_T) of pyrope calculated at different temperatures using the EoS parameters of

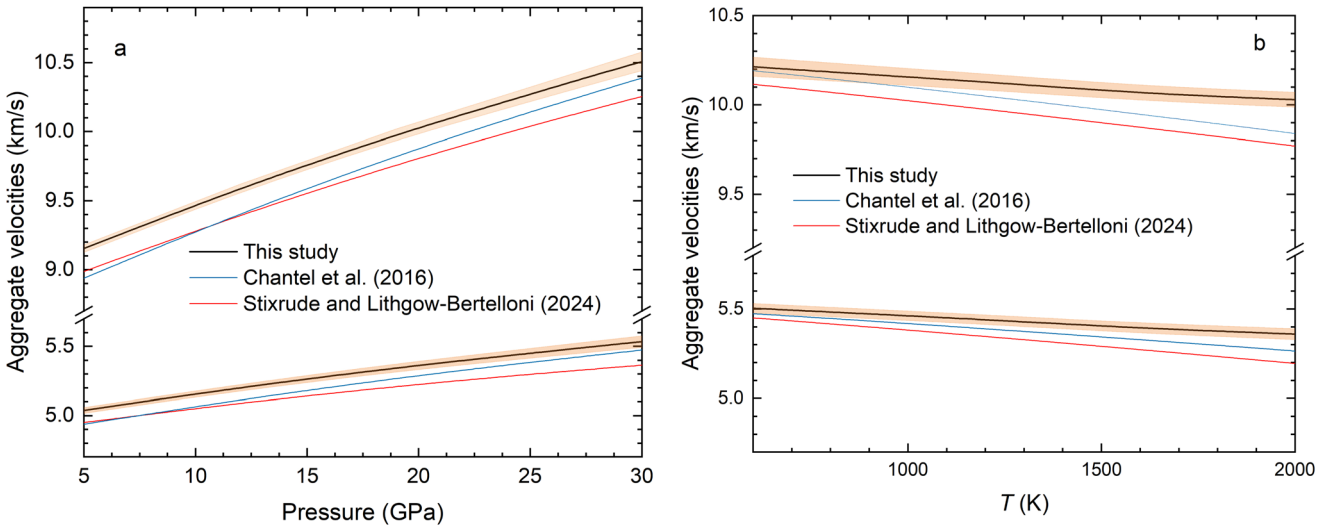

Fig. 11 Longitudinal and shear wave velocities calculated for pyrope using the EoS parameters derived in this study are compared with the models of Chantel et al. (2016) and Stixrude and Lithgow-Bertelloni (2024): **a**) as a function of pressure at mantle adiabatic temperatures (Katsura 2022) and **b**) as a function of temperature at 20 GPa

Angel et al. (2022) is compared with that calculated from the EoS determined in this study. The main differences arise from the slightly steeper dependence in pressure (i.e. higher K') and a larger decrease in K_T with temperature at lower pressures in the study of Angel et al. (2022). The higher K' is most likely inherited from ultrasonics data used in the fitting (Zou et al. 2012; Chantel et al. 2016), which have been discussed previously, whereas the lower K_T values are likely inherited from fitting the ambient pressure velocity data of Sinogeikin and Bass (2002), which only extend to 1073 K, whereas in our study data at approximately 3 GPa extend to 1598 K and reach 1923 K at 8.8 GPa. In summary, the agreement between our EoS and that of Angel et al. (2022) is extremely good at the conditions where this previous model could be fitted to actual data. This provides also an excellent benchmark for the results of the laser heated single-crystal technique.

In Fig. 11a the v_S and v_P wave velocities of pyrope are calculated as a function of pressure at temperatures along the mantle adiabat reported by Katsura (2022), but smoothed to remove the sharp jumps in temperature resulting from the latent heat of phase transformations occurring in the Earth's transition zone at approximately 14 GPa and 20 GPa. The values calculated from our study are compared with values determined using the global fit of Chantel et al. (2016) and the database of Stixrude and Lithgow-Bertelloni (2024). Pyrope is only one component in mantle garnet, which is comprised also of significant proportions of almandine and grossular and, depending on the pressure, majorite components. Pyrope remains one of the more dominant components over the garnet stability field, however, and existing measurements seem to indicate that EoS terms may be quite similar among the garnet components (Pamato et al. 2016; Beyer et al. 2021; Angel et al. 2022). As can be seen in Fig. 11a, the velocities calculated for pyrope using the database of Stixrude and Lithgow-Bertelloni (2024) are consistently below the values determined using our EoS, with deviations that increase with pressure and are outside of the uncertainties of our study. At the base of the transition zone (~24 GPa) the differences are approximately 200 m/s in v_P and 150 m/s in v_S. These differences can in part be attributed to lower values of q_0 and η_0 in our EoS (Table 2). The values obtained in our study, however, are fitted to data that extend to much higher temperatures than achieved in previous studies and, therefore, provide better constraints on these terms. It is quite possible that velocities for many mantle components are underestimated at mantle temperatures because high temperature data are lacking. This may explain why seismic velocities calculated for pyrolitic mantle compositions using mineral elasticity data are lower than seismic reference models in the lower half of the transition zone (Irifune et al. 2008; Pamato et al. 2016). This difference is larger in v_S but is also apparent in v_P. This discrepancy may in part be resolved if, as in the case of pyrope, velocities are generally higher at mantle adiabatic temperatures than so far reported.

A further consequence of the higher velocities determined in this study at high temperatures can be seen in Fig. 11b, where velocities are calculated as a function of temperature at 20 GPa, corresponding to approximately 570 km depth, near the base of the transition zone. At this depth, seismic velocities can be reproduced using the EoS parameters determined in this study for a mantle temperature of approximately 1850 K. The same values of seismic

wave velocities, however, can be obtained at temperatures 850 K lower for v_P and 750 K lower for v_S when the EoS parameters reported by Stixrude and Lithgow-Bertelloni (2024) are used. If variations in mantle velocities are to be interpreted in terms of mantle temperature or composition, it is critical to obtain more experimental data on the acoustic velocities of rock-forming mantle minerals at or near realistic mantle temperatures.

Acknowledgements The equipment for this research was supported through the ERC advanced grant number 227893 'DEEP' funded through the EU 7th Framework Program and the DFG grants FR1555/11 and MA4534/3-1. The research was supported by the funding grant KU 3447/1-1/2 from DFG. HM received funding through the European Union's Horizon 2020 research and innovation Programme (ERC grant 864877). We thank A. Withers for providing the Dora Maira sample, R. Njul for sample polishing and D. Wiesner for their assistance with the FIB device.

Author contributions AK, GC, TBB, HM and DJF contributed to the study conception and design. The HSW laser system was set up by AK, HM and GC, whereas the AA laser system was set up by AK, GC and TBB. Sample preparation and Brillouin scattering measurements were performed by AK, GC and TBB. Data analysis and thermoelastic models were performed by AK, GC, TBB and DJF. The first draft of the manuscript was written by AK and TBB and all authors commented and contributed to improve the manuscript. All authors read and approved the submitted manuscript.

Funding This study was funded by the ERC advanced grant number 227893 'DEEP' funded through the EU 7th Framework Program and the DFG grants FR1555/11, MA4534/3 – 1 and KU 3447/1–1/2.
Open Access funding enabled and organized by Projekt DEAL.

Data availability No datasets were generated or analysed during the current study.

Declarations

Competing interests The authors declare no competing interests.

References

Anderson WW (2019) An analytic expression approximating the Debye heat capacity function. AIP Adv 9(7). https://doi.org/10.1063/1.5110279

Andrault D, Fiquet G (2001) Synchrotron radiation and laser heating in a diamond anvil cell. Rev Sci Instrum 72(2):1283–1288. https://doi.org/10.1063/1.1343866

Andrault D, Fiquet G, Itié J-P, Richet P, Gillet P et al (1998) Thermal pressure in the laser-heated diamond-anvil cell: an X-ray diffraction study. Eur J Mineral 10:931–940

Angel RJ, Finger LW (2011) SINGLE: a program to control single-crystal diffractometers. Journal of Applied Crystallography, 44(1): 247–251. https://doi.org/10.1107/s0021889810042305

Angel RJ, Gilio M, Mazzucchelli ML, Alvaro M (2022) Garnet EoS: a critical review and synthesis. Contrib Miner Petrol 177:54. https://doi.org/10.1007/s00410-022-01918-5

Anzellini S, Boccato S (2020) A Practical Review of the Laser-Heated Diamond Anvil Cell for University Laboratories and Synchrotron Applications. Crystals, 10(6). https://doi.org/10.3390/cryst10060459

Aubaud C, Withers AC, Hirschmann MM, Guan Y, Leshin LA et al (2007) Intercalibration of FTIR and SIMS for hydrogen measurements in glasses and nominally anhydrous minerals. American Mineralogist, 92(5–6): 811–828. https://doi.org/10.2138/am.2007.2248

Bass JD, Anderson DL (1984) Composition of the Upper Mantle: Geophysical Tests of two Petrological Models. Geophysical Research Letters, 11(3): 229–232. https://doi.org/10.1029/gl011i003p00229

Beyer C, Kurnosov AV, Ballaran TB, Frost DJ (2021) High-pressure and high-temperature single-crystal X-ray diffraction of complex garnet solid solutions up to 16 GPa and 823 K. Phys Chem Miner 48(17). https://doi.org/10.1007/s00269-021-01139-5

Buchen J (2018) The elastic properties of wadsleyite and stishovite at high pressures. Ph.D. Thesis. Retrieved from https://epub.uni-bayreuth.de/4410/

Cammarano F, Romanowicz BA (2007) Insights into the nature of the transition zone from physically constrained inversion of long-period seismic data. Proc Natl Acad Sci USA 104:9139–9144

Chantel J, Manthilake GM, Frost DJ, Beyer C, Boffa Ballaran T et al (2016) Elastic wave velocities in polycrystalline $Mg_3Al_2Si_3O_{12}$-pyrope garnet to 24 GPa and 1300 K. American Mineralogist, 101(4): 991–997. https://doi.org/10.2138/am-2016-5335

Chen G, Cooke JAJ, Gwanmesia GD, Liebermann RC (1999) Elastic wave velocities of $Mg_3Al_2Si_3O_{12}$-pyrope garnet to 10 GPa. Am Mineral 84:384–388

Chopin C (1984) Coesite and pure pyrope in high-grade blueschists of the Western Alps: a first record and some consequences. Contrinution Mineralogy Petrol 86:107–118

Criniti G, Boffa Ballaran T, Kurnosov A, Liu Z, Glazyrin K et al (2024) Thermal equation of state and structural evolution of Al-Bearing Bridgmanite. J Geophys Research: Solid Earth 129(1). https://doi.org/10.1029/2023jb026879

Dewaele A, Fiquet G, Gillet P (1998) Temperature and pressure distribution in the laser-heated Diamond-Anvil cell. Rev Sci Instrum 69(6):2421–2426. https://doi.org/10.1063/1.1148970

Du W, Clark SM, Walker D (2015) Thermo-compression of pyrope-grossular garnet solid solutions: non-linear compositional dependence. Am Mineral 100:215–222. https://doi.org/10.2138/am-2015-4752

Duffy TS, Anderson DL (1989) Seismic velocities in Mantle Minerals and the Mineralogy of the Upper Mantle. J Phys Res 94:1895–1912. https://doi.org/10.1029/JB094iB02p01895

Goncharov AF, Zaug JM, Crowhurst JC (2005) Optical calibration of pressure sensors for high pressures and temperatures. J Appl Phys 97:094917. https://doi.org/10.1063/1.1895467

Gwanmesia GD, Zhang J, Darling K, Kung J, Li B et al (2006) Elasticity of polycrystalline pyrope (Mg3Al2Si3O12) to 9GPa and 1000°C. Physics of the Earth and Planetary Interiors, 155(3–4): 179–190. https://doi.org/10.1016/j.pepi.2005.10.008

Gwanmesia GD, Jackson I, Liebermann RC (2007) In search of the mixed derivative $\partial^2 M/\partial P \partial T$ (M = G, K): joint analysis of ultrasonic data for polycrystalline pyrope from gas- and solid-medium apparatus. Physics and Chemistry of Minerals, 34(2): 85–93. https://doi.org/10.1007/s00269-006-0130-x

Hartwig J, Galkin V (2021) Heat capacity, thermal expansion, and elastic parameters of pyrope. J Therm Anal Calorim 144:71–79. https://doi.org/10.1007/s10973-020-09396-2

Hess NJ, Schiferl D (1992) Comparison of the pressure-induced frequency shift of sm:YAG to the ruby and nitrogen vibron pressure scales from 6 to 820 K and 0 to 25 GPa and suggestions for use as a high-temperature pressure calibrant. J Appl Phys 71(5):2082–2086. https://doi.org/10.1063/1.351158

Immoor J, Marquardt H, Miyagi L, Speziale S, Merkel S et al (2020) An improved setup for radial diffraction experiments at high pressures and high temperatures in a resistive graphite-heated diamond anvil cell. Rev Sci Instrum 91:045121. https://doi.org/10.1063/1.5143293

Irifune T, Ringwood AE (1987) Phase Transformations in Primitive MORB and Pyrolite Compositions to 25 GPa and some Geophysical Implications. In: Manghnani, M.H., Syono, Y. (Eds.), High-Pressure Research in Mineral Physics: A Volume in Honor of Syun-iti Akimoto. Geophysical Monograph Series, pp. 231–242. https://doi.org/10.1029/GM039p0231

Irifune T, Higo Y, Inoue T, Kono Y, Ohfuji H, Funakoshi K (2008) Sound velocities of majorite garnet and the composition of the mantle transition region. Nature 451:814–817. https://doi.org/10.1038/nature06551

Kantor I, Prakapenka V, Kantor A, Dera P, Kurnosov A et al (2012) BX90: a new diamond anvil cell design for X-ray diffraction and optical measurements. Rev Sci Instrum 83(12):125102. https://doi.org/10.1063/1.4768541

Katsura T (2022) A revised adiabatic temperature profile for the mantle. J Geophys Research: Solid Earth 127. https://doi.org/10.1029/2021JB023562. e2021JB023562

King HE, Finger LW (1979) Diffracted Beam Crystal Centering and its application to high-pressure crystallography. J Appl Crystallogr 12:374–378. https://doi.org/10.1107/S0021889879012723

Kurnosov A, Marquardt H, Dubrovinsky L, Potapkin V (2019) A waveguide-based flexible CO_2-laser heating system for diamond-anvil cell applications. Comptes Rendus Geoscience, 351(2–3): 280–285. https://doi.org/10.1016/j.crte.2018.09.008

Li L, Long H, Raterron P, Weidner D (2006) Plastic flow of pyrope at mantle pressure and temperature. Am Mineral 91:517–525

Lu C, Mao Z, Lin J-F, Zhuravlev KK, Tkachev SN et al (2013) Elasticity of single-crystal iron-bearing pyrope up to 20 GPa and 750 K. Earth Planet Sci Lett 361:134–142. https://doi.org/10.1016/j.epsl.2012.11.041

Milani S, Nestola F, Alvaro M, Pasqual D, Mazzucchelli ML, Domeneghetti MC, Geiger C (2015) Diamond–Garnet Geobarometry: the role of garnet compressibility and expansivity. Lithos 227:140–147

Murakami M, Asahara Y, Ohishi Y, Hirao N, Hirose K (2009) Development of in situ brillouin spectroscopy at high pressure and high temperature with synchrotron radiation and infrared laser heating system: application to the Earth's deep interiorPhysics. Earth Planet Interiors 174:282–291. https://doi.org/10.1016/j.pepi.2008.07.030

Murakami M, Ohishi Y, Hirao N, Hirose K (2012) A perovskitic lower mantle inferred from high-pressure, high-temperature sound velocity data. Nature 485:90–95. https://doi.org/10.1038/nature11004

Nakatsuka A, Shimokawa M, Nakayama N, Ohtaka O, Arima H, Okube M, Yoshiasa A (2011) Static disorders of atoms and experimental determination of Debye temperature in pyrope: low- and high-temperature single-crystal X-ray diffraction study. Am Mineral 96:1593–1605. https://doi.org/10.2138/am.2011.3714

Pamato MG, Kurnosov A, Boffa Ballaran T, Frost DJ, Ziberna L et al (2016) Single crystal elasticity of majoritic garnets: Stagnant slabs and thermal anomalies at the base of the transition zone. Earth and Planetary Science Letters, 451: 114–124. https://doi.org/10.1016/j.epsl.2016.07.019

Ralph RL, Finger LW (1982) A Computer Program for Refinement of Crystal Orientation Matrix and Lattice constants from Diffractometer Data with Lattice Symmetry constraints. J Appl Crystallogr 15:537–539. https://doi.org/10.1107/S0021889882012539

Sandercock JR (1982) Trends in Brillouin scattering: studies of opaque materials, supported films, and central modes. In: Cardona M, Güntherodt G (eds) Light scattering in solids III. Topics in Applied Physics. Springer, Berlin, Heidelberg. https://doi.org/10.1007/3540115137_6

Sinogeikin SV, Bass JD (2000) Single-crystal elasticity of pyrope and MgO to 20 GPa by Brillouin scattering in the diamond cell. Phys Earth Planet Inter 120:43–62

Sinogeikin SV, Bass JD (2002) Elasticity of pyrope and majorite-pyrope solid solutions to high temperatures. Earth Planet Sci Lett 203:549–555

Skinner BJ (1956) Physical properties of end members of the garnet group. Am Mineral 41:428–436

Speziale S, Marquardt H, Duffy TS (2014) Brillouin scattering and its application in geosciences. Rev Mineral Geochem 78(1):543–603. https://doi.org/10.2138/rmg.2014.78.14

Stixrude L, Lithgow-Bertelloni C (2005) Thermodynamics of mantle minerals - I. Physical properties. Geophys J Int 162(2):610–632. https://doi.org/10.1111/j.1365-246X.2005.02642.x

Stixrude L, Lithgow-Bertelloni C (2024) Thermodynamics of mantle minerals – III: the role of iron. Geophys J Int 237:1699–1733. https://doi.org/10.1093/gji/ggae126

Trots DM, Kurnosov A, Vasylechko L, Berkowski M, Boffa Ballaran T et al (2011) Elasticity and equation of state of Li2B4O7. Physics and Chemistry of Minerals, 38(7): 561–567. https://doi.org/10.1007/s00269-011-0428-1

Trots DM, Kurnosov A, Ballaran TB, Tkachev S, Zhuravlev K et al (2013) The Sm:YAG primary fluorescence pressure scale. Journal of Geophysical Research: Solid Earth, 118(11): 5805–5813. https://doi.org/10.1002/2013jb010519

Weidner DJ, Ito E (1987) Mineral Physics Constraints on a Uniform Mantle Composition. In: Manghnani, M.H., Syono, Y. (Eds.), High-Pressure Research in Mineral Physics: A Volume in Honor of Syun-iti Akimoto. Geophysical Monograph Series, pp. 439–446. https://doi.org/10.1029/GM039p0439

Whitfield CH, Brody EM, Bassett WA (1976) Elastic moduli of NaCl by Brillouin scattering at high pressure in a diamond anvil cell. Rev Sci Instrum 47(8):942–947. https://doi.org/10.1063/1.1134778

Zhang JS, Bass JD (2016) Sound velocities of olivine at high pressures and temperatures and the composition of Earth's upper mantle. Geophys Res Lett 43(18):9611–9618. https://doi.org/10.1002/2016gl069949

Zhang JS, Bass JD, Gaohua Z (2015) Single-crystal Brillouin Spectroscopy with CO_2 laser heating and variable q. Rev Sci Instrum 86:063905. https://doi.org/10.1063/1.4922634

Zou Y, Irifune T, Gréaux S, Whitaker ML, Shinmei T et al (2012) Elasticity and sound velocities of polycrystalline Mg3Al2(SiO4)3 garnet up to 20 GPa and 1700 K. Journal of Applied Physics, 112(1). https://doi.org/10.1063/1.4736407